bound species fragmented during the multiple injection/thermalization cycles used to fill the ICR cell,[9] leaving primarily just M^+ atoms as the charged fragment.

In agreement with earlier ICR measurements[11] on C_{60}^+ and the other large even-numbered clusters of carbon, we found no reaction of the bare carbon cluster ions with such species as H_2, O_2, NO, and NH_3. Similar lack of reactivity was found with the $C_{60}La^+$ complex. In agreement with previous photofragmentation studies in a tandem time-of-flight (TTOF) apparatus,[12] ArF excimer laser (6.4 eV) irradiation of these bare clusters in the ICR trap produced fragmentation only as a result of high order multiphoton processes. As expected, the $C_{60}M^+$ clusters were nearly as photoresistant as C_{60}^+ itself.

Extreme photostability of C_{60}^+ and $C_{60}M^+$ was evident from the fact that no measurable dissociation occurred for any of these trapped clusters with less than 0.5 mJ cm^{-2} $pulse^{-1}$ even after over 30-s irradiation with the ArF excimer laser at 50 Hz. Estimates of the absorption cross section of C_{60} at this wavelength[13] indicate that the average such cluster absorbs roughly 300 ArF excimer photons during this period. Cooling by infrared emission between laser shots must therefore be very facile for such clusters.

However, at sufficiently high ArF excimer laser fluence per pulse both C_{60}^+ and the $C_{60}M^+$ complexes did begin to photodissociate. The fluence dependence of this process was roughly the same for the metal-containing complexes as measured previously in the TTOF experiments for the bare clusters.[12] For both, the primary photoprocess was observed to be C_2 loss to form the next smaller even-numbered cluster. Increasing either the laser pulse energy or the length of time the clusters were irradiated in the ICR trap resulted in extensive further dissociation, producing successively smaller even-numbered clusters.

As argued in the earlier TTOF study,[12] loss of C_2 from a carbon cluster is hard to understand *unless* that cluster is a closed, edgeless carbon cage. Otherwise it should lose the much more stable C_3. The linear chain and monocyclic ring clusters in the 2–30 carbon atom range[14] are known[12,15] to lose C_3, and graphitic sheets should also lose C_3. But for closed cages a concerted C_2 loss mechanism is likely to be the lowest energy process since only then can the next smaller even product form a closed cage.[12] The observation of C_2 rather than M^+ loss from $C_{60}M^+$ suggests that the metal ion is sterically bound, since a bond between K^+ or Cs^+ and carbon should be much weaker than a carbon–carbon bond. These results are then strong evidence that $C_{60}M^+$ clusters are composed of closed carbon cages with the metal ion trapped inside.

The endpoint of the C_2 loss process for bare clusters such as C_{60}^+ is known[12] to be C_{32}^+; it appears to be the smallest viable fragment cage. In this regard the corresponding behavior for the $C_{60}M^+$ complexes presented in Figure 1 is particularly interesting. For potassium–carbon clusters the smallest stable member in the even product ions is clearly seen in Figure 1 to be $C_{44}K^+$. For cesium the smallest fragment cluster is $C_{48}Cs^+$. These results are intriguing since breaks near these cluster sizes are predicted from a simple model which places an M^+ ion in the center of a closed carbon cage, allowing for the known ionic radius of M^+, a 1.65 Å van der Waals radius for each carbon atom, and C–C bond lengths in the range of 1.4–1.5 Å. Similar experiments with $C_{60}La^+$ photodissociation show breakoff to occur at $C_{44}La^+$ (or possibly $C_{42}La^+$), again nicely in accord with expectations for a central La^+ ion completely enclosed in an inert carbon cage.

Registry No. C, 7440-44-0; K, 7440-09-7; Cs, 7440-46-2; La, 7439-91-0.

(11) McElvany, W. N.; Baronovski, A. P.; Watson, C. H.; Eyler, J. R. *Chem. Phys. Lett.* **1987**, *134*, 214.
(12) O'Brien, S. C.; Heath, J. R.; Curl, R. F.; Smalley, R. E. *J. Chem. Phys.* **1988**, *88*, 220.
(13) Heath, J. R.; Curl, R. F.; Smalley, R. E. *J. Chem. Phys.* **1987**, *87*, 4236.
(14) Yang, S.; Taylor, K. J.; Craycraft, M. J.; Conceicao, J.; Pettiette, C. L.; Cheshnovsky, O.; Smalley, R. E. *Chem. Phys. Lett.*, submitted for publication.
(15) Geusic, M. E.; Jarrold, M. E.; McIlrath, T. J.; Freeman, R. R.; Brown, W. L. *J. Chem. Phys.* **1986**, *86*, 1986.

Probing Metal Cluster Formation in NaY Zeolite by ^{129}Xe NMR†

B. F. Chmelka, R. Ryoo,‡ S.-B. Liu,§ L. C. de Menorval,⊥ C. J. Radke,* E. E. Petersen, and A. Pines

Department of Chemistry and Chemical Engineering
University of California
Berkeley, California 94720
Materials and Chemical Sciences Division
Lawrence Berkeley Laboratory
Berkeley, California 94720
Received February 16, 1988

The performance of zeolite-supported metal catalysts is known to depend upon preparatory treatments.[1] Homogeneous and reproducible metal dispersion can be achieved only through careful control of calcination and reduction conditions, since migration and agglomeration of cluster precursors can occur with subsequent loss of catalytic activity.[2,3] In spite of considerable research,[4-9] the transformations undergone by metal guest species during calcination and reduction have not been established, primarily due to difficulties in characterizing chemical intermediates which exist as cluster precursors. By using the ^{129}Xe NMR spectroscopy technique pioneered by Fraissard and co-workers[10-13] and applied to recent advantage by us and others,[14-16] we gain insight into the detailed chemistry of metal–zeolite catalyst preparation. We report for the first time changes in the chemical environment of NaY-supported platinum guest species by monitoring shifts in the ^{129}Xe resonance signal induced by different chemical and thermal treatments.

Pt–NaY samples containing 15 wt % platinum were prepared by introducing the tetraammine salt, $Pt(NH_3)_4^{2+}$, into the zeolite lattice via the ion-exchange procedure of Gallezot et al.[2] The ion-exchanged Pt–NaY samples were dried in a vacuum oven overnight at 22 °C and then calcined in purified flowing oxygen at a heating rate of 11 °C/h to maximum temperatures ranging from 200 to 400 °C. Upon reaching the upper temperature limit, the furnace was turned off, allowing the insulated reactor to cool to 40 °C over a period of many hours. After evacuation for 10 h at 22 °C, xenon gas was introduced to various equilibrium pressures, guided by separate adsorption isotherm experiments.

* To whom correspondence should be addressed.
† Presented, in part, at the American Institute of Chemical Engineers national meeting in New York City, November 1987.
‡ Present address: Department of Chemistry, Korea Institute of Technology, 400 Kusong-dong, Chung-gu, Taejon-shi, Chung Chong nam-do, Korea.
§ Present address: Institute of Atomic and Molecular Sciences, Academia Sinica, P.O. Box 23-166, Taipei, Taiwan, R.O.C.
⊥ Present address: Laboratoire de Chimie Organique Physique et Cinetique Chimique Appliquées. VA 418 C.N.R.S., ENSCM, 8 rue Ecole Normale, 34075 Montpellier Cedex, France.

(1) Jacobs, P. A. *Stud. Surf. Sci. Catal.* **1982**, *12*, 71–85.
(2) Gallezot, P.; Alarcon, A.; Dalmon, J.-A.; Renouprez, A. J.; Imelik, B. *J. Catal.* **1975**, *39*, 334–349.
(3) Ribeiro, F. R.; Marcilly, C. *Geterog. Katl.* **1983**, *5*, 383–387.
(4) Jaeger, N.; Ryder, P.; Schulz-Ekloff, G. *Structure and Reactivity of Modified Zeolites*; Jacobs, P. A., et al., Eds.; Elsevier Science Publishers B.V.: Amsterdam, 1984; pp 299–311.
(5) Gallezot, P. *Catal. Rev.-Sci. Eng.* **1979**, *20(1)*, 121–154.
(6) Uytterhoeven, J. B. *Acta Phys. Chem.* **1978**, 53–69.
(7) Braun, G.; Fetting, F.; Haelsig, C. P.; Gallei, E. *Acta Phys. Chem.* **1978**, 93–97.
(8) Felthouse, T. R.; Murphy, J. A. *J. Catal.* **1986**, *98*, 411–433.
(9) Tzou, M. S.; Jiang, H. J.; Sachtler, W. M. H. *React. Kinet. Catal. Lett.* **1987**, *35(1–2)*, 207–217.
(10) Ito, T.; de Menorval, L. C.; Fraissard, J. P. *J. Chim. Phys. Phys.-Chim. Biol.* **1983**, *80*, 573–578.
(11) Ito, T.; Fraissard, J. P. *J. Chem. Soc., Faraday Trans. 1* **1987**, *83(2)*, 451–462.
(12) de Menorval, L. C.; Ito, T.; Fraissard, J. P. *J. Chem. Soc., Faraday Trans. 1* **1982**, *78*, 403–410.
(13) Fraissard, J.; Ito, T.; de Menorval, L. C.; Springuel-Huet, M. A. *Stud. Surf. Sci. Catal.* **1982**, *12*, 179–189.
(14) Ryoo, R.; Liu, S.-B.; de Menorval, L. C.; Takegoshi, K.; Chmelka, B.; Trecoske, M.; Pines, A. *J. Phys. Chem.* **1987**, *91*, 6575–6577.
(15) Scharpf, E. W.; Crecely, R. W.; Gates, B. C.; Dybowski, C. *J. Phys. Chem.* **1986**, *90*, 9–11.
(16) Shoemaker, R.; Apple, T. *J. Phys. Chem.* **1987**, *91*, 4024–4029.

0002-7863/88/1510-4465$01.50/0

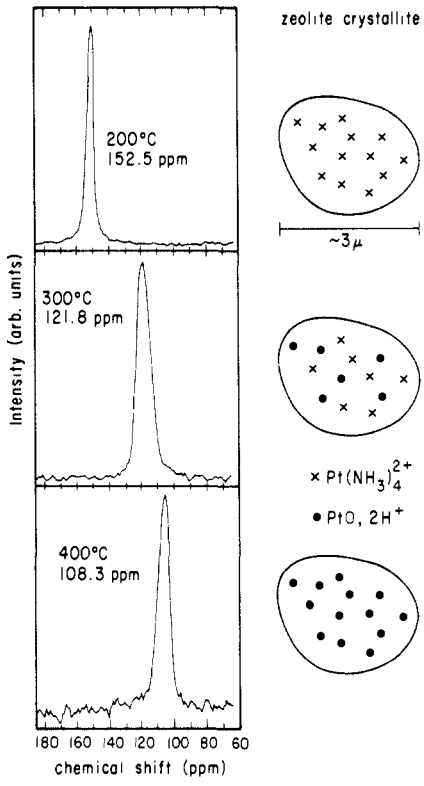

Figure 1. ^{129}Xe NMR spectra of xenon (equilibrium pressure 200 Torr, T = 22 °C) adsorbed in $Pt(NH_3)_4^{2+}$–NaY zeolite samples (ca. 15 wt % Pt) following calcination to 200, 300, and 400 °C. Accompanying the spectra are schematic diagrams depicting chemical differences in the metal species produced by the different thermal treatments. Upon removal of the platinum species' cationic charge during calcination, the anionic charge on the zeolite lattice is balanced by H^+ or NH_4^+ produced during decomposition of the metal–tetraammine complex.[18]

^{129}Xe NMR spectra of adsorbed xenon were obtained on a Bruker AM-400 spectrometer operating at 110.7 MHz. Typically, 2000–20000 signal acquisitions were accumulated for each spectrum with a recycle delay of 0.2 s between 90° pulses. Chemical shift measurements are precise to within 0.5 ppm and are expressed relative to xenon gas at very low pressure.[13] Following the different calcination treatments and ^{129}Xe NMR experiments, all samples were reduced in purified flowing hydrogen for 4 h at 400 °C. After evacuation for 10 h at 400 °C and cooling to ambient temperature, ^{129}Xe NMR spectra were obtained on the various reduced Pt–NaY samples as outlined above.

Figure 1 displays the room temperature ^{129}Xe NMR spectra of xenon adsorbed in the supercage cavities of $Pt(NH_3)_4^{2+}$–NaY zeolite samples calcined to different maximum temperatures. The single peak in each spectrum arises from motional averaging of the many locally distinct physisorption sites and xenon–xenon interactions which a xenon atom encounters during each signal acquisition. Accordingly, the ^{129}Xe chemical shift reflects the intrinsic perturbations experienced at each site, weighted by the collisional probability with which each interaction occurs. The ^{129}Xe chemical shift data indicate distinct chemical differences in the Pt–NaY samples resulting from different calcination treatments. For the specific case of adsorption under an equilibrium xenon pressure of 200 Torr, the ^{129}Xe chemical shift moves farther upfield in $Pt(NH_3)_4^{2+}$–NaY samples calcined to progressively higher temperatures. The heavy metal loading (ca. 2 Pt atoms/NaY supercage), coupled with enhanced xenon–Pt affinity,[10] makes ^{129}Xe NMR particularly sensitive to the nature of the metal guest and accounts for the large chemical shifts reported in Figure 1.

Chemical changes induced during the calcination process are apparent in Figure 2, where ^{129}Xe chemical shift data are plotted as a function of adsorbed xenon concentration for samples calcined to different maximum temperatures. The data clearly demonstrate the sizable differences in ^{129}Xe chemical shift behavior observed

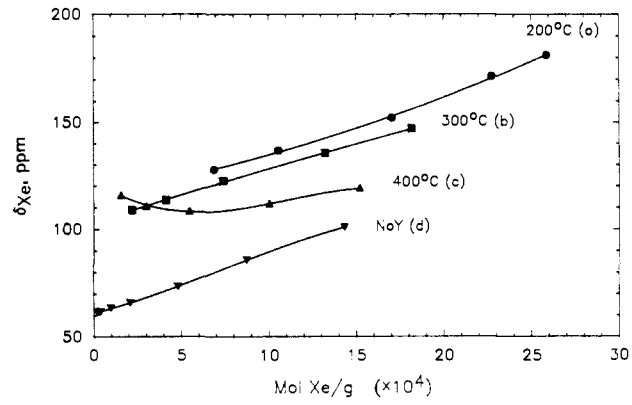

Figure 2. Variation in ^{129}Xe chemical shift with the concentration of adsorbed xenon (T = 22 °C) in $Pt(NH_3)_4^{2+}$–NaY zeolite samples calcined to 200, 300, and 400 °C. The ^{129}Xe resonance is isotropically averaged to a single peak in all spectra from which the above data are compiled. The chemical shift of ^{129}Xe adsorbed on NaY-zeolite dehydrated at 400 °C is shown for reference purposes in curve d.

for xenon adsorbed in samples possessing unique preparation histories. These chemical shift changes mirror a change in the average environment experienced by xenon atoms adsorbed within the supercages as a result of chemical changes undergone by the metal species during calcination. For more severe thermal treatments, the chemical shift of adsorbed ^{129}Xe decreases considerably for a given xenon uptake with the functional form of the plots becoming more curved as well.

At 200 °C, Figure 2a, the mild calcination treatment dehydrates the $Pt(NH_3)_4^{2+}$-exchanged zeolite without significant decomposition of the tetraammine complex. At higher calcination temperatures, Figure 2b,c, the tetraammine complex decomposes to a cluster precursor (most likely PtO) in which the platinum is shielded from interaction with adsorbed xenon atoms. The ^{129}Xe NMR data indicate the extent to which this decomposition has progressed and seem to rule out the presence of Pt^{2+} or autoreduced Pt as end products of the calcination process. Bare divalent cations and reduced metal species within zeolite supercages have previously been shown to have a much more pronounced effect on the chemical shift of the ^{129}Xe nuclear resonance.[11,12] At calcination temperatures above 500 °C, ^{129}Xe NMR, H_2 chemisorption, and transmission electron microscopy indicate decomposition of the cluster precursor with subsequent penetration of the metal species into sodalite cavities within the zeolite lattice.[17] Migration of metal species into the sodalite cavities has been observed at higher temperatures by Gallezot et al. (600 °C)[2] and Tzou et al. (550 °C).[9] Additional infrared spectroscopy data, high-resolution transmission electron micrographs, and ^{129}Xe NMR data supporting the identification of cluster precursor species will be presented in a full paper.

Following reduction of the samples, ^{129}Xe NMR data in Figure 3 show a dramatic dependence on the temperature of the earlier calcination. de Menorval et al. have previously documented large downfield shifts of the ^{129}Xe NMR signal in the presence of bare platinum clusters.[12] In separate H_2-chemisorption experiments, we find that the downfield shifts in the ^{129}Xe chemical shift data correlate well with the amount of surface platinum metal accessible within the zeolite supercages.[17] Accordingly, Figure 3c reflects a large fraction of surface platinum metal, while in curves a and b in Figure 3, the ^{129}Xe chemical shifts are substantially smaller, indicating smaller fractions of exposed platinum metal. For the sample calcined at 200 °C and reduced, high-resolution transmission electron micrographs reveal very large (ca. 40 nm in diameter) platinum clusters on the exterior of the micron-sized zeolite crystallites.[17] Accordingly, xenon adsorbed in predominantly empty NaY supercages in the crystallite's interior accounts for the low ^{129}Xe chemical shift values observed in Figure 3a. In

(17) Chmelka, B. F. Ph.D. Thesis, University of California-Berkeley, in progress.

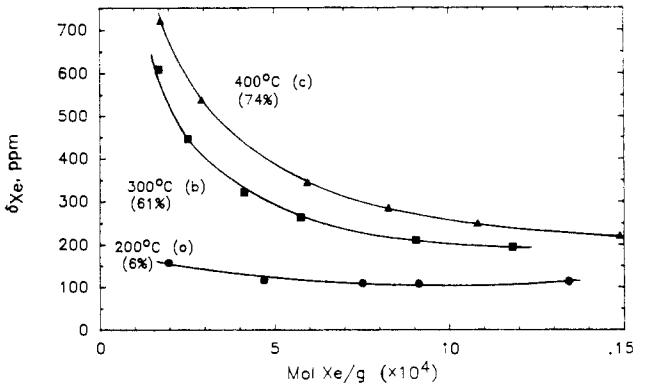

Figure 3. Variation in ^{129}Xe chemical shift with the concentration of adsorbed xenon (T = 22 °C) in reduced Pt–NaY zeolite samples previously calcined to different maximum temperatures (200, 300, and 400 °C). The percentage of surface platinum metal determined by hydrogen-chemisorption experiments is shown in parentheses for each sample.

summary, for the 400 °C reduction conditions imposed, ^{129}Xe NMR data indicate that formation of highly dispersed, NaY-supported platinum metal requires calcination at close to 400 °C and progresses through a shielded precursor species following decomposition of the metal–tetraammine salt.

These new ^{129}Xe NMR experiments represent a unique means of investigating metal–zeolite catalyst preparation and provide important insight into the chemistry of the calcination process. The sensitivity of physisorbed xenon to the influence of the metal guest makes ^{129}Xe NMR spectroscopy an important diagnostic probe of metal-clustering phenomena in zeolitic media.

Acknowledgment. This work was partially supported by the Director, Office of Energy Research, Office of Basic Energy Sciences, Material Sciences Division of the U.S. Department of Energy under Contract DE-AC03-76SF00098, by the National Science Foundation under Grant NSF 83-14564, and by a grant from the Shell Foundation.

(18) Reagan, W. J.; Chester. A. W.; Kerr, G. T. *J. Catal.* **1981**, *69*, 89–100.

Potential Dependence of the Conductivity of Poly(3-methylthiophene) in Liquid SO_2/Electrolyte: A Finite Potential Window of High Conductivity

David Ofer and Mark S. Wrighton*

Department of Chemistry
Massachusetts Institute of Technology
Cambridge, Massachusetts 02139

Received March 10, 1988

We wish to communicate the potential dependence of the conductivity of thiophene-derived polymers I and II confined to

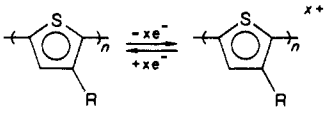

(1)

I R = CH_3
II R = H

Pt microelectrodes. The data show a broad maximum in conductivity as suggested by theory which shows a finite width for the highest occupied electronic bands.[1] The width of the region of high conductivity and the maximum conductivity are related because the bandwidth of the highest occupied band is a measure of the degree of delocalization in the system and can be roughly correlated with carrier mobility in the band.[1] It is known that oxidation of I or II, eq 1, leads to a dramatic increase in conductivity.[2] However, electrochemical studies of I and II[2,3] failed to reveal maxima in conductivity, possibly because chemical degradation of I and II occurs at positive potentials in the media used. The medium used for our new studies is liquid SO_2/0.1 M $[(n\text{-}Bu)_4N]PF_6$ at −40 °C. It has been demonstrated that liquid SO_2/electrolyte is a medium that allows observation of highly oxidized species.[4]

Previous work in this laboratory has shown that polyaniline does have a potential dependent conductivity in aqueous H_2SO_4[5] or in the solid electrolyte polyvinyl alcohol/H_3PO_4,[6] showing a well-defined maximum in conductivity at ~+0.3 V versus SCE and a region of high conductivity ~0.6 V wide. Bandwidths of polyaniline,[7] and polythiophene[1,8] have been calculated, but the results depend strongly on the structures assumed for the polymers. Such theoretical calculations should give reliable trends in bandwidth for structurally similar polymers. The calculations[1,7,8] suggest that a large fraction of the electrons in the highest occupied band might be electrochemically accessible in a number of polymers.

Arrays of eight individually addressable Pt microelectrodes (~2 μm wide, ~50 μm long, and ~0.1 μm high), separated from each other by ~1.2 μm,[3,5,9] can be coated and "connected" with I or II by anodic polymerization of the thiophene monomer in CH_3CN/0.1 M $[(n\text{-}Bu)_4N]PF_6$ as described by us[3] and earlier by others.[10] Two microelectrodes connected with a redox-active polymer can be used to determine the potential dependence of the conductivity of the polymer. At a fixed potential difference (drain voltage, V_D) between the two microelectrodes, the magnitude of the drain current, I_D, between the electrodes changes as the potential of the polymer, V_G, is changed.[3,5,9] Thus, I_D–V_G curves reveal the potential dependence of the conductivity, as reflected by I_D, of the polymer.

Figure 1 shows the scan rate dependence for cyclic voltammetry of I on a Pt microelectrode array in liquid SO_2/0.1 M $[(n\text{-}Bu)_4N]PF_6$ at −40 °C. Integration of the voltammogram indicates reversible removal of 9×10^{-8} mol of e⁻'s per cm² of area covered by polymer. We estimate that the oxidation process shown corresponds to removing one to two electrons per four repeat units of the polymer. At potentials negative of 0.6 V versus Ag, the features of the voltammogram correspond to those previously reported in other solvent/electrolyte systems.[2,3,10] In the region of more positive potential, new features, anodic and cathodic peaks at ~1.2 V and ~1.0 V versus Ag, respectively, are observed. The cyclic voltammetry over the entire region shown is qualitatively different than previously reported. Further work is required to establish the nature of the chemical changes accompanying the reversible removal of charge.

(1) Brēdas, J. L.; Elsenbaumer, R. L.; Chance, R. R.; Silbey, R. *J. Chem. Phys.* **1983**, *78*, 5656.

(2) (a) Tourillon, G. In *Handbook of Conducting Polymers*; Skotheim, T. A., Ed.; Marcel Dekker: New York, 1986; Vol. 1, Chapter 9. (b) Chandler, G. K.; Pletcher, D. In *Electrochemistry*; Pletcher, D., Ed.; Royal Society of Chemistry: London, 1985; Vol. 10, Chapter 3.

(3) Thackeray, J. W.; White, H. S.; Wrighton, M. S. *J. Phys. Chem.* **1985**, *89*, 5133.

(4) (a) Miller, L. L.; Mayeda, E. A. *J. Am. Chem. Soc.* **1970**, *92*, 5218. (b) Tinker, L. A.; Bard, A. J. *J. Am. Chem. Soc.* **1979**, *101*, 2316.

(5) Paul, E. W.; Ricco, A. J.; Wrighton, M. S. *J. Phys. Chem.* **1985**, *89*, 1441.

(6) Chao, S.; Wrighton, M. S. *J. Am. Chem. Soc.* **1987**, *109*, 6627.

(7) (a) Boudreaux, D. S.; Chance, R. R.; Wolf, J. F.; Shacklette, L. W.; Brēdas, J. L.; Thēmans, B.; Andrē, J. M.; Silbey, R. *J. Chem. Phys.* **1986**, *85*, 4584. (b) Stafström, S.; Brēdas, J. L. *Synth. Met.* **1986**, *14*, 297.

(8) (a) Thēmans, B.; Andrē, J. M.; Brēdas, J. L. *Synth. Met.* **1987**, *21*, 149. (b) Riga, J.; Snauwaert, Ph.; De Pryck, A.; Lazzaroni, R.; Boutique, J. P.; Verbist, J. J.; Brēdas, J. L.; Andrē, J. M.; Taliani, C. *Synth. Met.* **1987**, *21*, 223.

(9) (a) Kittlesen, G. P.; White, H. S.; Wrighton, M. S. *J. Am. Chem. Soc.* **1984**, *106*, 7389. (b) White, H. S.; Kittlesen, G. P.; Wrighton, M. S. *J. Am. Chem. Soc.* **1984**, *106*, 5375.

(10) (a) Tourillon, G.; Garnier, F. *J. Electroanal. Chem.* **1982**, *135*, 173. (b) Tourillon, G.; Garnier, F. *J. Electroanal. Chem.* **1983**, *148*, 299. (c) Waltman, R. J.; Bargon, J.; Diaz, A. F. *J. Phys. Chem.* **1983**, *87*, 1459.

0002-7863/88/1510-4467$01.50/0